Q. J. R. Meteorol. Soc. (2004), **130**, pp. 295–323 doi: 10.1256/qj.02.226

The dynamics of a midlatitude cyclone with very strong latent-heat release

By F. AHMADI-GIVI, G. C. GRAIG and R. S. PLANT*
University of Reading, UK

(Received 8 December 2002; revised 30 June 2003)

SUMMARY

The role of latent-heat release in an explosively developing cyclone from the Fronts and Atlantic Storm-Track Experiment is examined within the potential vorticity (PV) framework. Using conventional synoptic analysis, piecewise PV inversion and numerical simulations, the development is described in terms of an upper-level PV (UPV) anomaly, a surface potential-temperature anomaly and diabatically generated PV anomalies in the lower and upper troposphere. The relative contributions of each anomaly to the cyclogenesis are investigated, along with the interactions between anomalies.

In contrast to previous case-studies, the results of PV inversion and sensitivity tests reveal that the contribution from the surface thermal anomaly is much weaker than those associated with the upper-level and diabatically generated PV anomalies. A low-level PV (LPV) anomaly is generated rapidly in response to the UPV anomaly, and dominates the intensification of the system, but its associated circulation has only a modest feedback effect on the upper levels. However, diabatic reduction of PV in the upper troposphere is found to have important effects on the UPV anomaly. In particular, latent heating tends to destroy the UPV anomaly by inhibiting its downward penetration and reducing its horizontal extent.

KEYWORDS: Cyclogenesis FASTEX Potential-vorticity inversion

1. INTRODUCTION

The baroclinic cyclone is the most common phenomenon on synoptic scales in midlatitudes, and has been a focus of meteorological research for many decades. A great number of theoretical studies and case-studies have specifically investigated the effects of diabatic processes on baroclinic dynamics (e.g. Danard 1964; Tracton 1973; Gyakum 1983a,b; Emanuel *et al.* 1987; Kuo *et al.* 1991a,b; Davis and Emanuel 1991; Reed *et al.* 1993; Stoelinga 1996), and it is generally agreed that release of latent heat is the most important such process, particularly in the most severe maritime cyclones.

Theoretical studies (e.g. Emanuel *et al.* 1987; Craig and Cho 1988; Snyder and Lindzen 1991; Montgomery and Farrell 1991; Whitaker and Davis 1994; Balasubramanian and Yau 1994, 1996) have consistently shown that latent-heat release will increase the growth rates of baroclinic instabilities, while decreasing the horizontal scale of the region of ascent. However, the structure of the disturbance remains broadly similar to that of a dry baroclinic instability, unless the magnitude of the latent-heat release is very large. Some studies (Craig and Cho 1988; Snyder and Lindzen 1991; Parker and Thorpe 1995) have found that strong diabatic energy conversions can dominate over baroclinic processes, and that the structure of the disturbance then changes so that it is confined to the region of latent-heat release. Apparently, the diabatic heating can provide a dynamical surrogate for the basic-state baroclinicity and produce a 'moist' baroclinic instability even in situations that are stable in the absence of heating (Snyder and Lindzen 1991; Craig and Cho 1992). These results suggest that in some cases moist baroclinic instability is not necessarily the result of a cooperative interaction between the diabatic heating and dry baroclinic processes, but rather that the presence of heating introduces distinct effects that may compete with the dry processes. However, these linear studies used a highly simplified parametrization for latent-heat release, and the extent to which their results can be applied to the more complex dynamics of real cyclones is unclear.

* Corresponding author: Department of Meteorology, University of Reading, PO Box 243, Reading, Berkshire RG6 2BB, UK. e-mail: r.s.plant@rdg.ac.uk

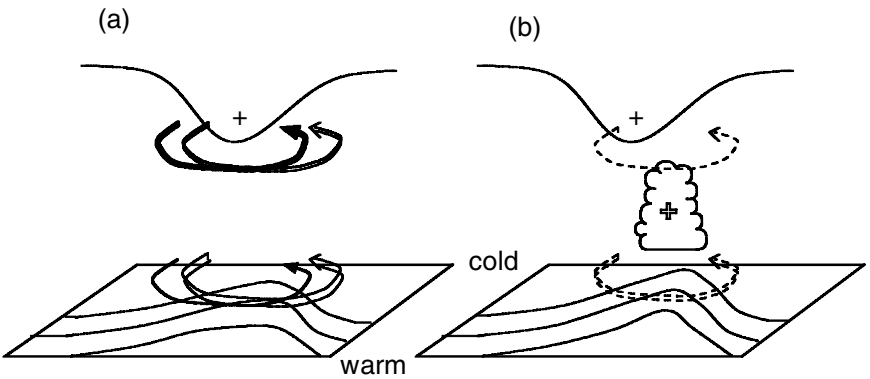

Figure 1. (a) Schematic illustration of circulations associated with upper-level potential-vorticity (PV) and surface potential-temperature anomalies, acting to reinforce each other. The upper line illustrates a tropopause fold, with associated positive PV anomaly and corresponding circulations denoted by solid arrows. Potential-temperature contours are shown on the surface, with the corresponding circulations denoted by open arrows. (Adapted from Hoskins *et al.* (1985)). (b) Illustrates with dotted arrows the circulations associated with a diabatically produced positive PV anomaly.

An attractive approach for investigating the role of latent-heat release in observed cyclones is the potential-vorticity (PV) framework. As discussed in the seminal paper of Hoskins *et al.* (1985), PV is conserved in the inviscid, adiabatic processes of baroclinic instability, while diabatic heating produces sources and sinks of PV. The invertibility principle allows the balanced part of the flow to be derived from the PV distribution, along with the potential-temperature distribution at the earth's surface.

Many case-studies have made use of the invertibility principle in order to examine the contributions of upper- and lower-level PV anomalies to low-level cyclones, and to investigate how the anomalies interact. Results from such analyses can be divided into two broad categories, according to whether the impact of any diabatically produced PV anomaly on the baroclinic dynamics was weak or strong. For systems in the weak category, cyclogenesis is primarily driven by baroclinic dynamics, with latent-heat release playing a secondary role (e.g. Hoskins and Berrisford 1988; Davis and Emanuel 1991; Davis *et al.* 1993; Fehlmann and Davies 1998; Huo *et al.* 1999). This situation is shown schematically in Fig. 1, adapted from the classic picture of baroclinic instability in Hoskins *et al.* (1985). The primary effect of latent-heat release is to produce a positive PV anomaly in the lower troposphere, located above, or a little upshear (Stoelinga 1996), of the surface warm anomaly. The cyclonic circulation associated with the diabatic PV anomaly tends to reinforce that of the surface warm anomaly and also to enhance the upper-level and surface anomalies through advection (Fig. 1(b)). The growth of the disturbance is enhanced without dramatically changing its structure. Latent-heat release can also produce a negative PV anomaly in the upper troposphere (not shown in Fig. 1) that can reinforce the upper-level ridge downstream of the cyclone centre. However, the effects of this negative anomaly appear to be less significant (Pomroy and Thorpe 2000).

The validity of this simple picture, however, is questionable for the category in which latent-heat release makes a strong contribution to the intensity of the surface cyclone. This is particularly true for cases in which surface thermal gradients are weak (e.g. Craig and Cho 1992; Reed *et al.* 1993; Stoelinga 1996). Indeed, Craig and Cho (1992) speculated that the low-level, diabatically produced PV anomaly was able to act as a substitute for the absent surface warm anomaly. Instability would occur since the upper-level anomaly would induce ascent that would lead to latent-heat release and

the intensification of the low-level anomaly. The low-level anomaly would in turn induce a cyclonic circulation that would enhance the upper-level anomaly by advection. In a case-study, Stoelinga (1996) found substantial advection of upper-level PV by winds associated with diabatically produced PV in the lower troposphere. Note also that in cases of strong diabatic PV production in the lower troposphere, it would seem plausible that the correspondingly strong diabatic reduction in upper-level PV might also prove to be important.

In this study we investigate whether or not a particular intense extratropical cyclone was produced predominantly through the interaction of an upper-level PV anomaly with a diabatically produced, low-level anomaly. The interactions of various PV anomalies are considered, including the effects of PV reduction in the upper troposphere. The cyclone studied is an explosively developing event from the Fronts and Atlantic Storm-Track Experiment (FASTEX) that exhibited intense cumulus convection throughout its life cycle, indicating that latent-heat release was likely to have been strong. The investigation is presented as follows. Section 2 describes the data and methodology used, while section 3 introduces the event with a synoptic overview. The relative importance of individual PV anomalies is examined in section 4 and their interactions are considered in section 5. Our conclusions are presented in section 6.

2. Data and methodology

(*a*) *Data*

FASTEX was an international meteorological field experiment, which took place during January and February 1997. The observing system included a temporally enhanced network of radiosonde stations in western Europe, seven research aircraft and four ships to provide dropsonde, radiosonde and other observations with high resolution (see Joly *et al.* (1997) and Clough *et al.* (1998) for more information).

The case chosen for this study was the subject of FASTEX intensive observing period IOP18. IOP18 covered the life cycle of the cyclone, beginning at 0000 UTC 22 February 1997 and ending at 0000 UTC 24 February 1997. The main reasons for choosing this case are firstly, the existence of widespread and intense convection throughout the cyclone development and secondly, the successful forecast of the cyclone by the Met Office limited area model (LAM). The presence of intense convection indicates that condensation, and therefore the release of latent heat, may be an important feature of the cyclogenesis. The ability to produce a good LAM forecast is vital because sensitivity tests using the LAM form an important part of this study. One indicator of the forecast quality is shown in Fig. 2, which compares the three-hourly minimum surface pressures from an objective analysis and from a control experiment with the LAM. The analysis data used here is a model-assimilated set (Macpherson *et al.* 1996), obtained using the LAM. Some other indicators of the successful LAM forecast can be found in Clough *et al.* (1998, Table 7).

(*b*) *The methodology*

A combination of approaches is applied to study the processes involved in the development of the IOP18 cyclone, and in particular the role of latent-heat release. In addition to a conventional synoptic analysis, diagnostic analyses of assimilated data are performed using piecewise PV inversion, and some numerical simulations are investigated. The PV inversion scheme followed and some general characteristics of the simulations are described below.

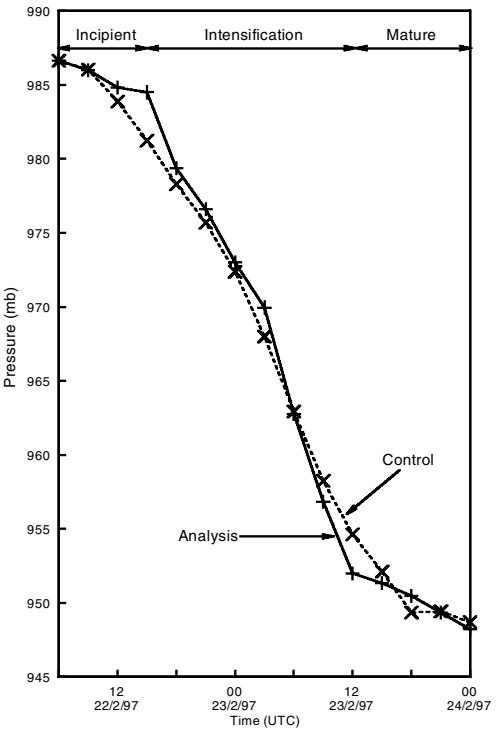

Figure 2. Time series of the minimum surface pressure in the IOP18 cyclone at 3 h intervals. The series labelled 'analysis' is taken from analysis data at 6 h intervals and from T+3 forecasts at intermediate times. The series labelled 'control' is obtained from a 42 h control simulation (specifically, CON2 from Table 2). Three distinct stages of development have been identified from the series, and are indicated at the top of the figure.

(i) *PV inversion.* This study makes extensive use of piecewise PV inversion to attribute aspects of the circulation to particular features in the PV field, allowing the evolution of the flow to be interpreted in terms of interactions between different PV anomalies (Davis and Emanuel 1991; Bishop and Thorpe 1994). The PV inversion system used has previously been described by Griffiths *et al.* (2000). It is based on the full Ertel–Rossby PV and determines the non-divergent wind field associated with a PV distribution by means of the Charney (1955) nonlinear balance equation. Clearly, the extent to which the inversion can reproduce the observed winds depends upon the accuracy of this imposed dynamical balance. In order to estimate the importance of neglecting the irrotational part of winds in the nonlinear balance equation, the differences between the observed and balanced (non-divergent) winds have been examined. For example, during the main period of intensification*, the greatest departures from balance are ~20% at 850 mb and ~10% at 400 mb. Such departures correspond to centres of low-level convergence and upper-level divergence, with balance being satisfied to good accuracy elsewhere. While significant, departures on this scale indicate that the balanced, non-divergent wind is nevertheless able to capture the main features of the flow.

In order to avoid numerical problems due to unstable lapse rates in the planetary boundary layer, the PV inversion domain has been restricted to the range 900–50 mb. For this reason, in the context of the PV inversion calculations, the term 'surface potential-temperature anomaly' will actually refer to a surrogate anomaly on the 900 mb

* Specifically, at 0600 UTC 23 February 1997.

level. The lateral boundary conditions used for solving the equations are identical to those of Davis and Emanuel (1991). On the upper and lower boundaries, either Neumann or Dirichlet boundary conditions may be applied. In practice, however, it has been found that the wind and temperature fields attributed to PV anomalies are almost identical in the two cases (Ahmadi-Givi 2001). The results presented in this paper are taken from inversions with potential temperature held fixed on the horizontal boundaries.

The contribution from an individual PV anomaly is determined by comparing two successive PV inversions. The first uses the full PV field to find the full balanced wind and potential-temperature fields. The second inversion is for a modified PV field, with the relevant anomaly removed. Fields attributed to the PV anomaly are then obtained from the difference between the two sets of fields. Any piecewise inversion scheme introduces errors due to the fundamental nonlinearity of PV inversion. For instance, in this scheme the sum over the geopotential perturbations attributed to each component of the full PV field will not produce the balanced perturbation obtained by inverting the full field. While the scheme may be modified to impose this property (as in Davis 1992; Davis *et al.* 1993), the uncertainties due to nonlinearity are not removed, merely transformed, by such a procedure. An important point for the reliability of our results is that nonlinear effects are assumed to be tolerably small for spatially distinct anomalies, as argued by Birkett and Thorpe (1997).

A second source of ambiguity lies in the definitions used for the PV anomalies themselves. The definitions are required reliably to identify perturbations of interest in situations where they may be superimposed upon strong gradients or embedded within complex and evolving background fields. Three different approaches towards anomaly definition have been explored within this study, referred to here as the 'temporal average', 'spatial average' and 'objective' methods. It should be stressed that we do not regard any one of these approaches as being intrinsically superior to any of the others, although, of course, a particular method may prove to be more convenient for a given application. Instead, we regard the differences between results obtained with the three approaches as providing some useful measure of the fundamental uncertainty involved in specifying the anomalies. Therefore, we would argue that our PV-inversion analysis is robust, in the sense that inferences drawn from the analysis are known not to be qualitatively sensitive to the method used for specifying anomalies.

In all cases, an anomaly is defined by subjectively determining the region that contains the anomaly and then within that region, subtracting some background field from the original one. Such a scheme, using localized anomalous regions, has been followed by Griffiths *et al.* (2000) and Pomroy and Thorpe (2000), for example. The three approaches vary in the choice of background and, also, in whether or not the subtraction is applied for all points within the region. A temporal-average method is perhaps the most common choice of background (e.g. Davis and Emanuel 1991; Davis 1992; Stoelinga 1996) and defines the background PV field to be a time mean of the PV over the lifetime of the system of interest. A spatial-averaging method takes the background to be a spatially averaged value for each vertical level at each time, and is often convenient for isolating anomalies within the lower troposphere, where gradients of PV are relatively small. For both cases, the subtractions apply throughout the designated anomalous region. Finally, in an objective method, one defines a bounding value for PV. Any larger values (if one is considering a positive anomaly, say) within the anomalous region are reset to the bounding value.

In this study, the IOP18 dynamics are interpreted in terms of the interactions of upper- and lower-level PV anomalies, along with a surface potential-temperature anomaly. The PV anomalies are distinct, isolated regions of unusually high PV centred

in the upper and lower troposphere, respectively. Thus, the upper-level PV (UPV) anomaly is essentially just the positive part of the upper-level anomalous PV. Although one can identify a potentially important negative anomaly at upper levels, downstream of the UPV anomaly, we find that the negative anomaly is strongly influenced by the presence of latent heating. Thus, we have preferred to treat this downstream ridge as a separate entity, which is discussed in section 5(b).

It remains to describe the detailed methods used to define the anomalies in the inversion calculations presented here. Although other approaches were also tested, as outlined above, it is not desirable to describe the similar sets of results obtained using each method. Instead, we refer the interested reader to Ahmadi-Givi (2001) for comparisons of some of the different methods. The UPV anomaly is defined using the temporal-averaging approach. However, unlike Davis and Emanuel (1991), say, we do not use the mean over the whole lifetime of the system. As shown in section 3, the UPV anomaly in this case appears within a broad region of high-PV values associated with a large-scale, slowly moving upper trough. Averaging over the complete life of the cyclone (several days) smooths out the large-scale structure as well as the localized anomaly of interest that is directly associated with the IOP18 cyclone. A shorter time period (two days) is therefore used in order to obtain a background, mean-PV field that retains the broad trough. (The averaging was applied between 0000 UTC 22 February and 0000 UTC 24 February 1997.)

Spatial averaging is used to define the low-level PV (LPV) anomaly. This is straightforward, since this LPV anomaly is a highly localized region of diabatically generated, high PV within a background of fairly uniform lower PV values.

At early times, gradients of potential temperature in the vicinity of the IOP18 cyclone are weak, and the surface thermal (θ_B) anomaly is most easily identified with a temporal-averaging approach. In fact, it turns out that the θ_B anomaly remains rather weak throughout the IOP18 lifetime (section 4). If one uses the maximum size of the attributable geopotential perturbation in order to measure the strength of an anomaly, then the temporal-averaging approach tends to underestimate the strength of a thermal anomaly in comparison with, say, an objective approach. This is because the thermal anomaly defined by temporal averaging includes both cold and warm anomalies*, whereas an objective approach can be used to isolate only the warm anomaly. In order to demonstrate our claim that the thermal anomaly remains a weak contributor to IOP18 intensification, we choose to present results that err in the sense of overestimating its contribution. Thus, an objective method is used which excludes only the high temperatures in the vicinity of the surface cyclone.

(i) *The limited-area model.* The LAM, version 4.4, is used for the control experiments and sensitivity tests. It is a part of the Unified Model (Cullen 1993) and is described by Panagi and Dicks (1997). The LAM domain covers Western Europe, the North Atlantic and the eastern coast of the United States and Canada. It uses a rotated spherical latitude/longitude co-ordinate system and has its computational north pole at 30°N, 160°E. This means that the equator of the computational grid passes roughly through the centre of the domain and so produces a roughly even grid spacing in distance. The horizontal resolution is 0.4425° in latitude and longitude, or ≈50 km. In the vertical, 19 levels are used, with a hybrid σ-pressure coordinate. The vertical resolution ranges from 50 m in the layer adjacent to the surface to over 2 km within the stratosphere.

* Since warm and cold thermal anomalies are separated by fronts, it is not feasible to choose a region that includes the full extent of the warm anomaly without also enclosing a significant amount of cold anomaly.

Boundary conditions imposed on the LAM are derived from previous global model forecasts.

3. Synoptic overview

The evolution of the minimum surface pressure during IOP18 is shown in Fig. 2. Three distinct stages in the development of the surface cyclone are apparent, and have been marked on the figure. During the incipient and mature stages, the surface pressure decreases with time, but does so only slowly. By contrast, in the intermediate intensification stage, development is rapid, the surface pressure falling by 33 mb over 21 h.

The synoptic situation during the incipient stage is illustrated by Fig. 3(a), an infrared satellite image for 0000 UTC 22 February. At this time, the incipient cyclone may be distinguished by a small mass of convective cloud over the Labrador Sea (labelled A). This cloud feature is located within a region of positive vorticity advection ahead of an upper-level, short-wave trough which is found on the upstream side of a major large-scale trough. Figure 4(a) shows the height of the 2 PVU surface for this time. The short-wave trough can be seen as a structure with particularly low tropopause height (as little as ~2.7km) around 55°N, 53°W. We also note a second region of convection within the cold air mass (labelled B in Fig. 3(a)), which is located further east. Boundaries of the cold air mass are marked by two cloud bands labelled as F1 and F2. F1 represents a deep, synoptic-scale baroclinic zone with a broad band of moderately deep cloud. It corresponds to the main warm conveyor belt (WCB) in the conceptual model of Harrold (1973). F2, meanwhile, is an old polar-front cloud band, related to the IOP17 cyclone (Clough *et al.* 1998).

Towards the end of the incipient stage, at 1200 UTC 22 February, the cold-air feature A has intensified somewhat and moved eastward (Fig. 3(b)). A new development during the incipent stage is the formation of an additional cloud feature (labelled C), visible between A and B. A sequence of infrared satellite pictures (not shown) indicates that this prominent disturbance is formed and grows quickly in response to the rapid east-south-eastward motion of the short-wave trough. At later times, it is found that the feature A neither intensifies nor increases in size, and there is no clear evidence of it during intensification. During the incipient stage there is also no apparent interaction between A and F1, and the surface charts reveal no closed contours of the 4 mb isobars. Inspection of PV fields on isentropic surfaces at three-hourly intervals indicates that the structure and intensity of the short-wave trough do not evolve significantly during the incipent stage. Moreover, during this stage there are no noticeable features (such as low-level PV anomalies or significant fronts) that can be related to diabatic PV production in the lower troposphere or thermal advection at the surface.

Nonetheless, an early sign of the coming intensification can be seen in Fig. 3(b). A mid-level cloud extrusion (labelled W2) appears on the cold side of F1. It first appears as a bulge on F1 at the beginning of the intensification stage but later expands and increases in depth (as indicated by a higher brightness in the infrared images). The band W2 corresponds to the secondary WCB in the conceptual model of Young *et al.* (1987). It is formed from low-level air near the cyclone centre and includes some air originating from the lower part of the WCB F1, which peels off towards the cyclone centre. Bader *et al.* (1995) stated that the emergence of a W2 cloud feature is a sign that cyclogenesis is proceeding.

As development continues, W2 appears to rotate cyclonically and to approach the cold-air feature C. As shown in Fig. 3(c), these two cloud features start to merge

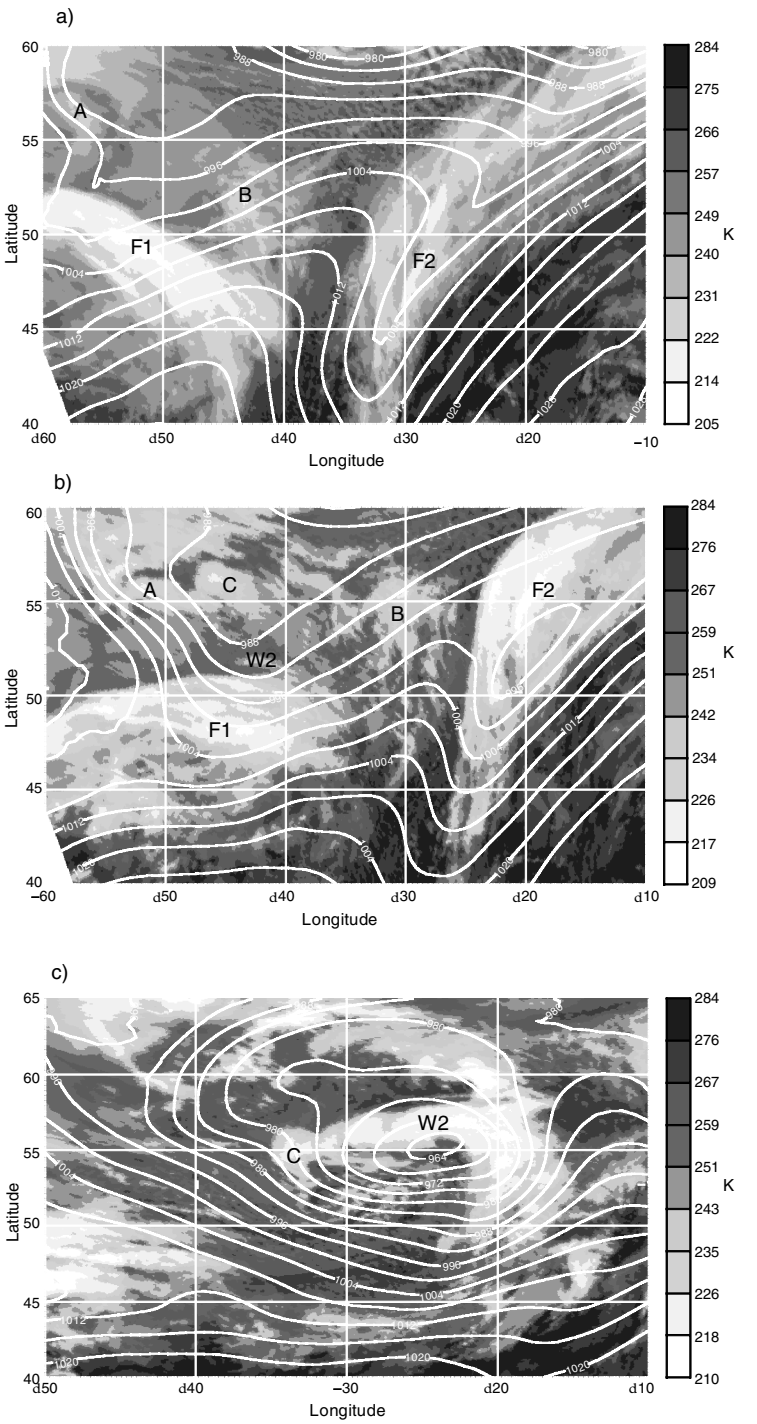

Figure 3. Meteosat infrared satellite images of the North Atlantic region overlaid with mean-sea-level pressure contours at 4 mb intervals for: (a) an early time (0000 UTC 22 February), (b) towards the end of the incipient stage (1200 UTC 22 February), and (c) during the intensification stage (0600 UTC 23 February). The temperature scale of the cloud tops is shown on the right of each panel. Letters mark cloud features that are discussed in the text.

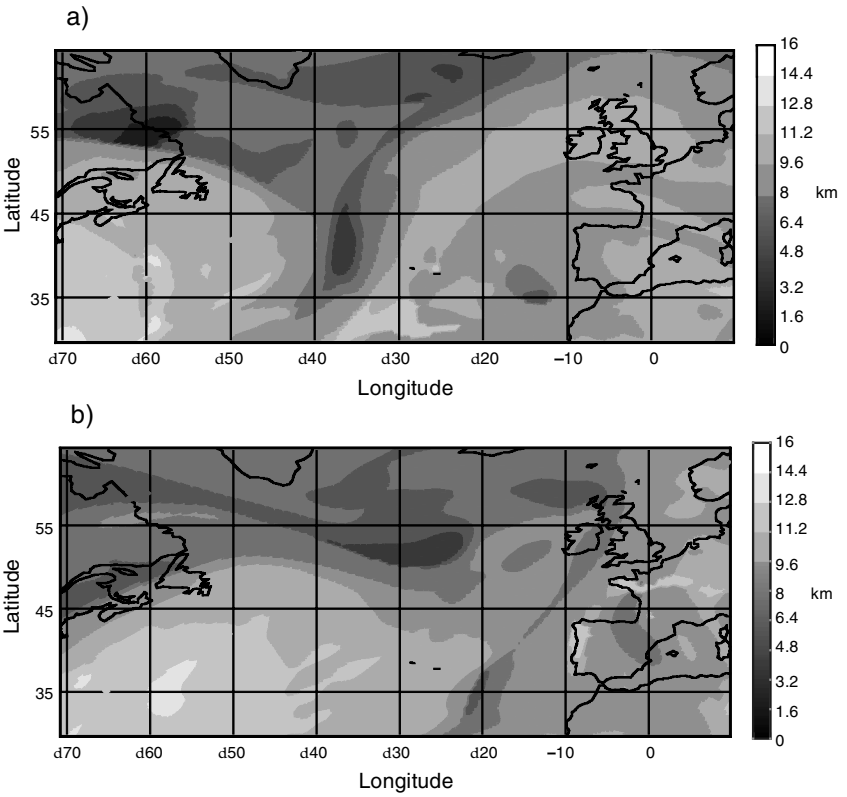

Figure 4. Height of the 2 PVU surface for: (a) 0000 UTC 22 February, and (b) 0600 UTC 23 February 1997. The height scale is shown on the right of each panel.

around 0600 UTC 23 February and combine to form a comma-head-like shape. Large numbers of convective clouds exist within the merging region at this time. Browning (1995) has stated that vigorous ascent of a W2 flow typically results in large amounts of precipitation in the region of the cloud extrusion corresponding to the cloud head. Following the merger a significant surface low develops, centred below the southern edge of the combined cloud mass. By 1200 UTC 23 February the two cloud features become indistinguishable on satellite images, as cloud-top temperatures associated with the W2 feature decrease to values similar to those of the cold-air feature. The most rapid deepening of the surface low occurs between 0300 and 0900 UTC 23 February (Fig. 2) during and immediately following the merger.

Coincident with the emergence of the W2 feature during intensification, a low-level PV anomaly develops, reaching a value of ~2 PVU at 0600 UTC 23 February (Fig. 5). The region of PV generation coincides with a region where model analyses indicate significant precipitation. Thus, although low-level PV anomalies can sometimes be generated by the action of friction within a region of strong baroclinicity (Davis *et al.* 1993; Stoelinga 1996; Adamson 2001), this particular anomaly would appear to be diabatically generated through the release of latent heat. (In section 4(b) a numerical simulation is described in which latent heating is excluded from the model. In that case, the low-level PV anomaly does not develop.) It would be expected that diabatic formation of this positive PV anomaly would also be accompanied by corresponding PV destruction at upper levels (Reed *et al.* 1992; Persson 1995; Stoelinga 1996; Wernli

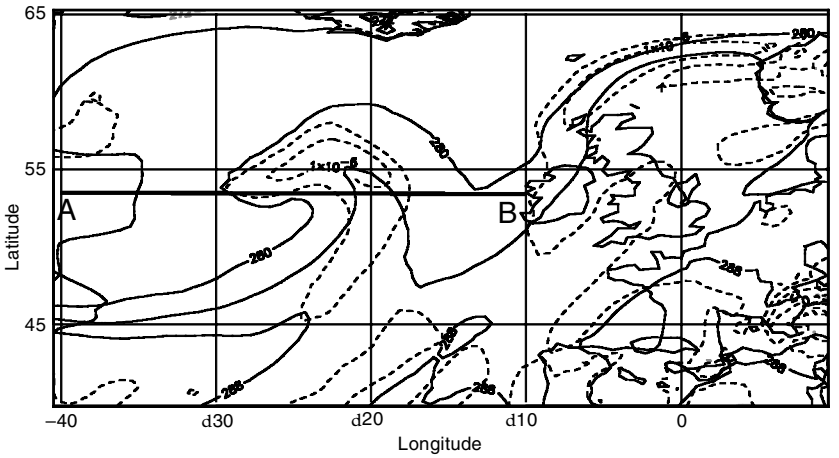

Figure 5. Potential temperature at 900 mb (solid lines, contour interval 4 K), overlaid with PV at 850 mb (dashed lines, contour interval 0.5 PVU) for 0600 UTC 23 February 1997. The line AB shows the location of the east–west cross-section in Fig. 6(d).

and Davies 1997a,b; Pomroy and Thorpe 2000). As discussed in section 5(b), such destruction results in a negative anomaly of PV downstream of the upper-level short-wave trough.

The short-wave trough (UPV anomaly) moves eastward relative to the large-scale upper-level trough and also begins to rotate cyclonically. As the cloud features merge on 0600 UTC 23 February, the UPV anomaly is situated on the base of the large-scale trough (Fig. 4(b)). The magnitude of the PV within this anomaly (not shown) is somewhat weaker than at earlier times, but its position at the axis of the large-scale trough, together with the low PV values that have developed in the downstream ridge, lead to a more intense UPV anomaly relative to its immediate environment.

A small-scale wave, denoting enhanced thermal advection, can first be distinguished in the low-level potential-temperature charts at 1800 UTC 22 February (not shown). The wave intensifies over time and reaches its maximum amplitude within 12 h. Figure 5 shows the contours of potential temperature at 900 mb for 0600 UTC 23 February when the thermal wave is at its most pronounced. The temperature gradients at both the cold and warm fronts are rather weak, reaching ~3 K per 100 km across the cold front. For comparison, in Kuo *et al.* (1992) a thermal gradient greater than 10 K per 100 km is reported near the low centre during the mature stage. Fronts of similar strength have also been found in a number of other explosive extratropical cyclones (for example, those described by Shapiro and Keyser (1990), Davis and Emanuel (1991) and Reed *et al.* (1992)).

The mature stage of the IOP18 cyclone is characterized by a wrapping of the cloud band and the dry intrusion (associated with stratospheric PV values) around the low centre. PV anomalies at all levels begin to weaken after achieving their maximum values at the end of the intensification stage.

The synoptic analysis suggests that the pre-existing, upper-level, short-wave UPV anomaly may play an important role in initiating cyclogenesis. Both a surface thermal anomaly and a low-level, diabatically generated PV anomaly are developed, and may themselves contribute significantly to the cyclogenesis during the intensifying stage.

The relative contributions of each anomaly to cyclone development are considered in the next section.

4. Relative contribution of PV anomalies

(*a*) *PV inversion*

With anomalies of PV and surface potential-temperature defined as in section 2(b), inversions have been performed for each anomaly every six hours throughout the IOP18 period. In much of the following discussion we will characterize the contribution of each anomaly to the cyclone by the maximum perturbation in the attributed geopotential-height field at 850 mb. (Similar approaches*, based on the relative sizes of geopotential-height perturbations, have been followed by Balasubramanian and Yau (1994), Stoelinga (1996), Huo *et al.* (1999) and others.) The pressure surface chosen is located within the PV-inversion domain, but is close enough to the ground to represent the main features of the surface cyclogenesis.

A typical example of the piecewise PV-inversion results is shown in Fig. 6 for 0600 UTC 23 February, a time when the cyclone is intensifying rapidly. East–west cross-sections are shown for the geopotential-height perturbations attributed to each of the three anomalies considered. Each cross-section passes through the maximum 850 mb geopotential perturbation for the anomaly in question. Also shown (Fig. 6(d)) is the total height perturbation, constructed by summing the perturbations attributed to each of the inverted anomalies. Clearly the UPV anomaly is the dominant contributor at upper levels, but its influence weakens somewhat at lower levels. The LPV and θ_B anomalies are associated with significant geopotential-height perturbations at low levels but these contributions decay quite quickly with increasing height. Examples of the horizontal structures of the attributed height and wind fields can be found in Ahmadi-Givi (2001). They exhibit little horizontal structure of interest since the PV anomalies are smaller than the radius of deformation.

Figure 7 shows the evolution of the attributed 850 mb maximum geopotential-height perturbations. The results extend from the incipient stage to the mature stage of development. During the incipient stage, the UPV anomaly is the dominant contributor. The LPV anomaly plays a lesser, but nevertheless a significant, role while the effect of the θ_B anomaly is almost negligible. Some amplification of the perturbations induced by the UPV and θ_B anomalies occurs in the intensification stage. A much more pronounced change, however, is the strong intensification of the fields attributed to the LPV anomaly. The contribution from this anomaly becomes comparable to that from the UPV anomaly at the end of the intensification phase.

As discussed in section 2(b), the uncertainty inherent in defining PV anomalies means that alternative definitions should be investigated in order to provide sensitivity checks. Such checks support the above description of the relative contributions from the three anomalies and their patterns of evolution. Moreover, we note that an alternative attribution analysis using the quasi-geostrophic omega equation (following Clough and Davitt (1994)) has also been conducted. The results are described by Ahmadi-Givi (2001). This analysis also leads to similar conclusions regarding the relative importance

* While we examine the perturbation maxima for each individual contribution, some authors have preferred to consider instead the contributions at the point of the total perturbation maximum. The alternative approach would lead to reductions in our quoted height perturbations in the range ~5–15 m (Fig. 6). Relative individual contributions would not change by more than ~10 m, which is insufficient to change our results at a qualitative level (Fig. 7). The significance of the relative positions of the individual maxima is discussed by Plant *et al.* (2003).

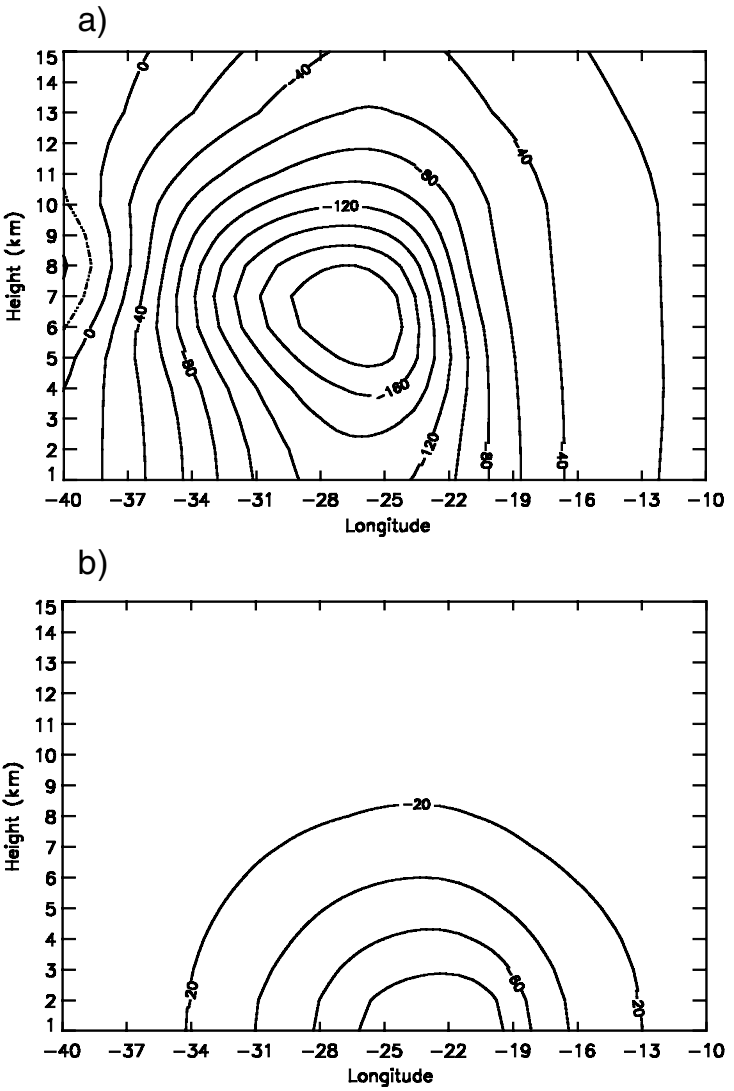

Figure 6. East–west cross-sections of the geopotential-height perturbations attributed to various PV anomalies at 0600 UTC 23 February. The cross-sections are drawn through the latitude where the 850 mb geopotential-height perturbation has its maximum value for the anomaly (or combination of anomalies) in question. Results for: (a) the UPV anomaly along 52.3° N, (b) the LPV anomaly along 55.5° N, (c) the θ_B anomaly along 52.5° N, and (d) the sum of the three anomalies along 54.2° N. The location of the cross-section in (d) is denoted by line AB in Fig. 5. The contour interval in (a), (b) and (d) is 20 m, while that in (c) is 10 m. Negative perturbations are shown with solid lines and positive perturbations with dashed lines.

of contributions from different levels in the atmosphere. Thus, it constitutes another valuable check on the reliability of our PV-inversion methods.

(*b*) *Numerical experiments*

The static PV inversions described above show the relative importance of each anomaly for a sequence of specified times. Although this is certainly useful information, the possibilities for interactions between anomalies mean that a sequence of inversions

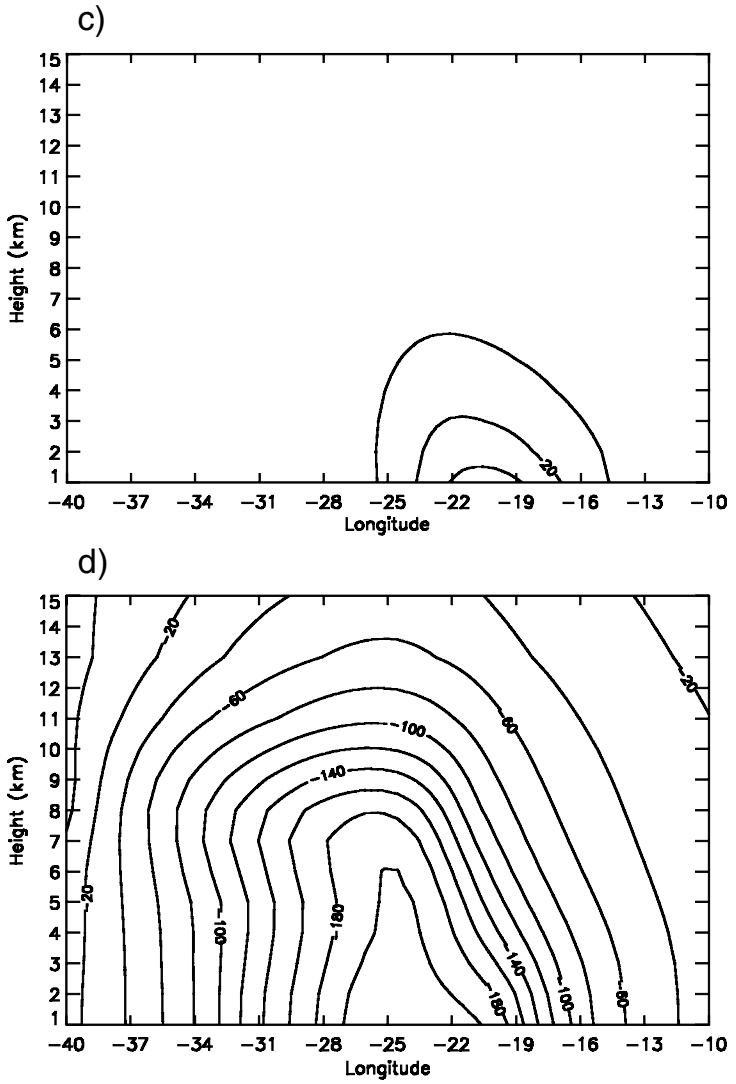

Figure 6. Continued.

may not be sufficient to provide the complete picture of the cyclogenesis. For instance, although the contribution from some particular anomaly might consistently prove to be instantaneously weak, it is nonetheless possible that the anomaly plays a crucial role in the development of the system via its influence on other anomalies. If only for this reason, it is useful to supplement the PV inversion results above by investigating some numerical experiments in which anomalies are removed from the initial model atmosphere. Two sets of experiments are considered (Tables 1 and 2).

The first set of experiments (summarized by Table 1) is run for 24 h. The experiments are initialized midway through the intensification stage, specifically at 0000 UTC 23 February. By this time, all of the anomalies have been developed. A control experiment with full physics and unmodified initial data (CON1) provides a basis for comparison. Three sensitivity experiments have been performed in order to test the

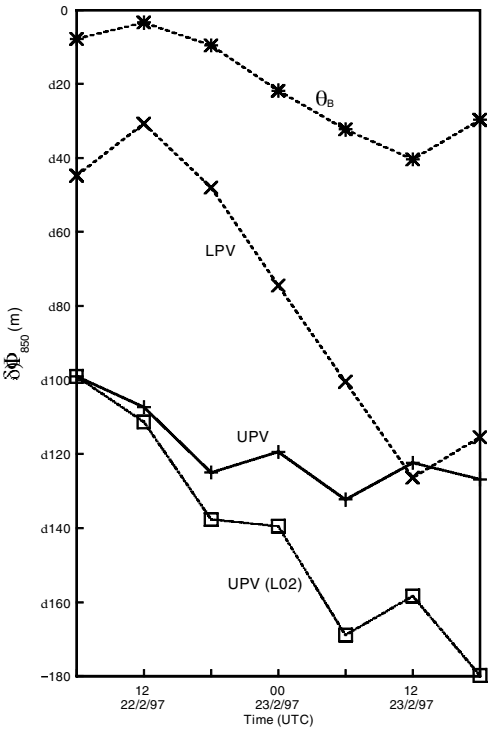

Figure 7. The maximum geopotential-height perturbations at 850 mb from the upper-level PV anomaly (UPV), the diabatically produced PV anomaly (LPV), the surface thermal anomaly (θ_B), and the upper-level PV anomaly in experiment L02, without latent heating (UPV(L02)).

TABLE 1. EXPERIMENTS INITIALIZED AT 0000 UTC 23 FEBRUARY AND INTEGRATED FOR 24 H

Experiment	UPV anomaly	LPV anomaly	θ_B anomaly	Latent heating	Surface fluxes	Description
CON1	Yes	Yes	Yes	Yes	Yes	Control
MUP1	No	Yes	Yes	Yes	Yes	No UPV anomaly at T+0
MLP	Yes	No	Yes	Yes	Yes	No LPV anomaly at T+0
MT0	Yes	Yes	No	Yes	Yes	No θ_B anomaly at T+0
L01	Yes	No	Yes	No	Yes	No latent-heat release
LS01	Yes	No	Yes	No	No	No latent heating or surface fluxes

See text for further explanation.

TABLE 2. EXPERIMENTS INITIALIZED AT 0600 UTC 22 FEBRUARY AND INTEGRATED FOR 42 H

Experiment	UPV anomaly	LPV anomaly	θ_B anomaly	Latent heating	Surface fluxes	Description
CON2	Yes	Yes	Yes	Yes	Yes	Control
MUP2	No	Yes	Yes	Yes	Yes	No UPV anomaly at T+0
L02	Yes	No	Yes	No	Yes	No latent-heat release
LS02	Yes	No	Yes	No	No	No latent heating or surface fluxes

See text for further explanation.

impact on subsequent cyclogenesis of removing each of the anomalies from the initial conditions of the model. For these experiments, all other model options and parameters were kept identical to those of the control simulation. The experiments are referred to as MUP1 (UPV anomaly removed, using temporal averaging), MLP (LPV anomaly removed, using spatial averaging) and MTO (θ_B anomaly removed, using the objective method).

Two other experiments are listed in Table 1 and have been included for further investigation of the LPV anomaly. In L01 the LPV anomaly is removed from the initial conditions as in MLP. However, in this case it is prevented from redeveloping by setting to zero the latent heat of condensation. An LPV anomaly might also be affected by surface heat fluxes, followed by turbulent transport through the boundary layer into the free troposphere. In the LS01 experiment therefore, both surface heat fluxes and latent-heat release were excluded from the model run.

The second set of experiments is summarized in Table 2 and ran for 42 h, starting during the incipient phase of cyclone development at 0600 UTC 22 February. This period covers both the triggering of the cyclone and the major phase of its development. At the initial time, the short-wave UPV anomaly is clearly in evidence, but there are as yet no significant LPV or θ_B anomalies. Thus, there were no experiments in the second set analogous to MLP and MTO from the first set. All other first-set experiments have direct analogues in the second set.

Some additional experiments have been carried out to check that the results are not overly sensitive to the way in which the PV anomalies in the initial conditions are defined. For example, if the UPV anomaly is identified by spatial (rather than temporal) averaging then inversion of the anomaly produces a similar flow. Moreover, the subsequent evolution of the numerical experiment is little altered. Removal of the θ_B anomaly with temporal (rather than objective) averaging has a rather more significant effect, producing an initial state with some noticeable differences in structure (see section 2(b)). However, because of the small influence (cf. Fig. 7) and rapid regeneration (see later) of the θ_B anomaly the subsequent development of the cyclone is essentially unchanged.

Figure 8 presents the minimum surface pressures obtained from the control and sensitivity experiments listed in Table 1. The simulation results support the conclusions obtained from the sequence of piecewise PV-inversion calculations (Fig. 7). In particular, the sensitivity of the cyclogenesis to removal of the θ_B anomaly (MTO) is very small in comparison with the large changes that occur if the UPV anomaly is removed (MUP1) or if latent heating is excluded (L01). Indeed, if latent heating is excluded then a significantly weaker cyclone is formed. This confirms the crucial role of diabatic heating for the intensification of the IOP18 system.

Both the simulation results from L01 and the synoptic analysis in section 3 indicate that the LPV anomaly is formed mainly by latent-heat release. However, if the LPV anomaly is removed at the initial time (MLP), then the pressure of the mature cyclone at T+24 is found to be somewhat weaker but does not change dramatically. The minimum surface pressure in the MLP experiment follows that in the no-latent-heat experiment L01 for several hours (Fig. 8), but the LPV anomaly can be quickly and almost completely regenerated by latent heating. Hence, later intensification is considerably stronger in MLP than in L01. Apparently, the LPV anomaly in IOP18 is continuously being renewed, rather than built up gradually over the life of the cyclone. We note that the same property has been observed in some other cases (Stoelinga 1993; Pomroy and Thorpe 2000) and defer further discussion of this regeneration to section 5. By contrast, a comparison of the L01 and LS01 experiments reveals that surface heat fluxes

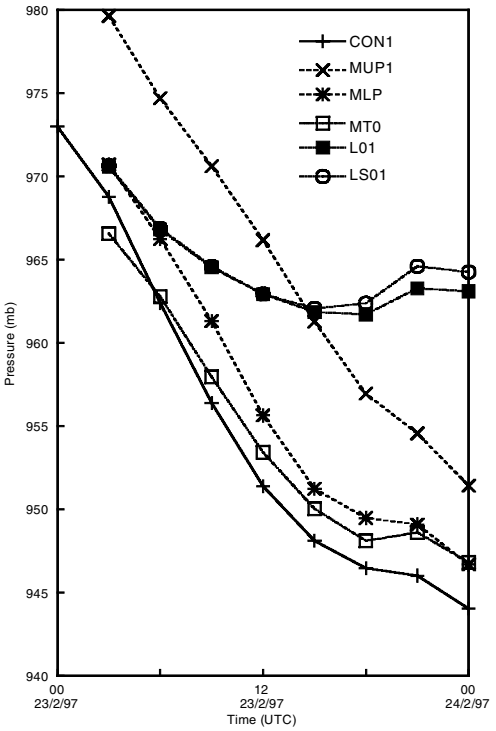

Figure 8. Time series at three-hour intervals of the minimum surface pressure of the IOP18 cyclone in control and sensitivity simulations. Each simulation is labelled by an identifer. The identifiers are listed in Table 1.

during the intensification stage have only a weak impact on the LPV anomaly and on the deepening of the surface cyclone (Fig. 8).

If the UPV anomaly is removed midway through intensification (MUP1), then the initial value of surface pressure is considerably increased but intensification is found to proceed at a comparable rate (Fig. 8). This provides another indication that the development of the LPV anomaly appears to be the main process driving the deepening of the system during the intensification stage. A UPV anomaly is found in the MUP1 experiment, but it remains significantly weaker than that seen in the control experiment (CON1) at the same time. The generation of a UPV anomaly in MUP1 may perhaps be partly due to the unavoidably imperfect isolation of the initial UPV anomaly. However, the continued descent and southward advection of stratospheric air is also responsible for producing the anomaly. The reasons for this advection are discussed in section 5.

The cyclogenesis of IOP18 appears quite different to the interaction of PV anomalies in cyclones dominated by baroclinic instability, where the surface low is associated with UPV and θ_B anomalies that intensify as the system develops. In IOP18 the θ_B anomaly appears to play almost no role, the UPV anomaly does not intensify, and the deepening of the surface low is due mainly to the generation of an LPV anomaly by latent-heat release. However, the LPV anomaly does not gradually accumulate over time, but rather appears to form as a residual of rapid processes of generation and destruction (generation is sufficiently rapid to renew the anomaly within $\sim$6 h). Moreover, although the UPV anomaly contributes significantly to the system strength (Fig. 7), any development of that anomaly does not contribute significantly to the intensification.

5. Interaction between PV anomalies

The conventional picture of baroclinic instability is of UPV and θ_B anomalies acting to reinforce each other by advection across the gradients of the background flow. This picture would not appear to provide a good description for the intensification of IOP18 (section 4). Below we consider some interesting features of the interactions between anomalies for this case.

(*a*) *Influence of UPV anomaly on low-level anomalies*

First consider the role of the UPV anomaly in the generation of the LPV and θ_B anomalies. The synoptic analysis of section 3 indicates that the cyclone is triggered by a UPV anomaly that crossed the Labrador coast at 0000 UTC 22 February. However, the intensification phase of surface cyclogenesis does not begin until some 15 h later (Fig. 2). PV inversions reveal that at early times the circulation associated with the UPV anomaly is not ideally placed to create a low-level thermal anomaly. Figure 9 shows the circulation attributed to the UPV anomaly at 900 mb, overlaid with the potential-temperature field on that level, for times before and during the intensification stage. Prior to intensification (Fig. 9(a)) the induced circulation lies somewhat north-west of the main east–west, low-level fronts. Advection of warm, moist air is therefore rather modest. Although something of a warm anomaly has developed around 60°N, 55°W, the high temperatures are relatively low and little moisture is available at this time. However, by 0600 UTC 23 February (Fig. 9(b)), the UPV anomaly has moved south-eastward, approaching a warmer region of stronger temperature gradients and drawing a warm tongue of moist, subtropical air towards the north. The role of the UPV anomaly in creating the θ_B perturbation is confirmed by experiment MTO, in which the θ_B anomaly is removed from the initial state. Comparison with CON1 indicates that the warm anomaly is regenerated quickly and attains magnitudes very close to those in the control experiment after ~6 h of simulation. Note that the circulation associated with the developing LPV anomaly also contributes to warm advection during the intensification stage. A comparison of the L01 and MUP1 experiments suggests that, towards the end of the intensification stage, the UPV and LPV anomalies are of comparable importance in acting to generate a thermal anomaly.

As noted in section 4(b), the LPV anomaly is also regenerated quickly after being removed from the initial state (the MLP experiment). This can be seen in Fig. 10 which compares the 850 mb PV in the CON1 and MLP experiments after 12 h of integration. Clearly the LPV anomaly in MLP has developed rapidly (Fig. 10(b)), attaining a strength only slightly less than the anomaly in CON1 (Fig. 10(a)). In order to investigate the effects of surface heat fluxes in regenerating the LPV anomaly, the MLP experiment was repeated without such fluxes. This resulted in a 10–15% reduction in the magnitude of the LPV anomaly (not shown). Thus, the modest effect of surface heat fluxes, together with the weak circulations attributed to the θ_B anomaly, suggest that the LPV anomaly is generated mainly by the condensation of moisture within the ascending air, the available moisture having previously been advected northwards during the incipent stage by the winds attributed to the UPV anomaly.

(*b*) *Influence of latent heating and the low-level anomalies on upper-level anomalies*

While it is clear that the UPV anomaly plays a crucial role in developing the LPV and θ_B anomalies, the nature of the feedback from these anomalies to the upper-level structure is perhaps less obvious. More generally, in addition to the formation of the LPV anomaly, the action of latent-heat release can affect the upper-level PV in a number of

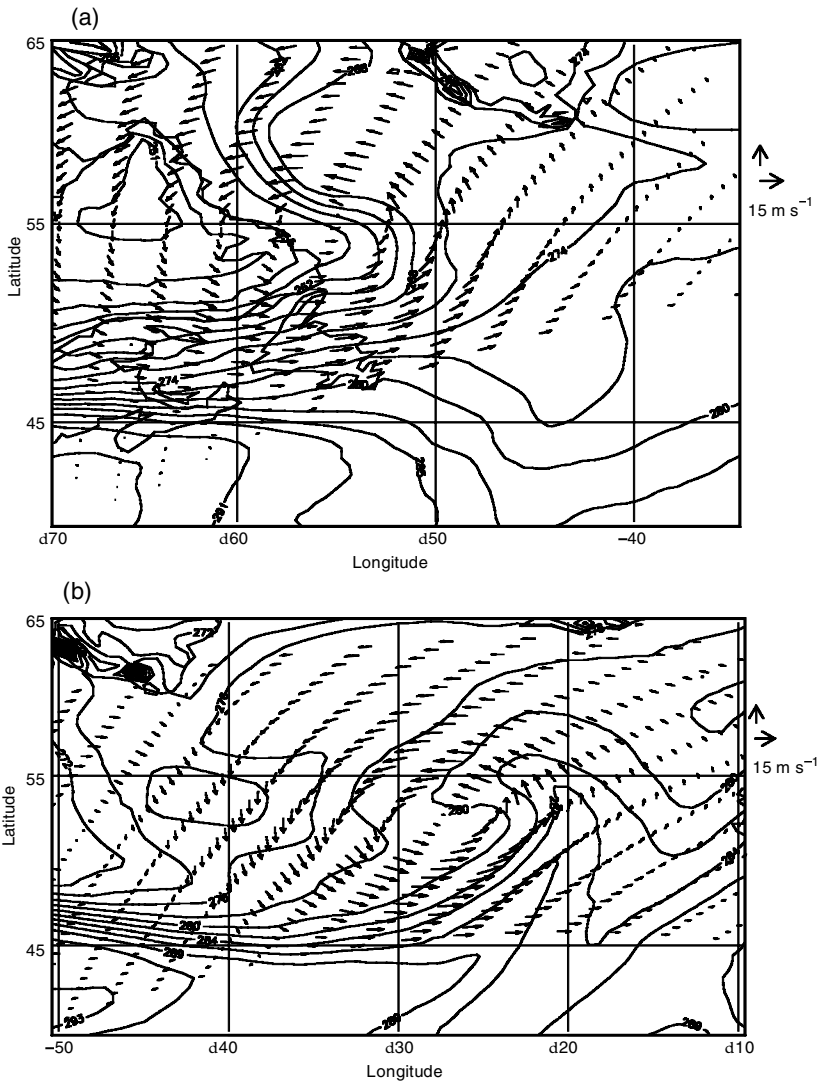

Figure 9. Winds at 900 mb attributed to the upper-level potential-vorticity anomaly overlaid with potential-temperature contours on that level for (a) 0600 UTC 22 February and (b) 0600 UTC 23 February 1997. The scale for the wind vectors is shown by the arrows to the right, denoting winds of 15 m s^{-1}. The potential-temperature contour interval is 3 K.

ways. Clearly, the balanced upper-level advection attributed to the LPV anomaly may act to redistribute upper-level PV. There is also the possibility of advective feedback from the surface thermal anomaly. However, latent-heat release can also produce a direct, diabatic reduction of upper-level PV, as noted in section 1. Another consideration is the PV redistribution associated with divergent outflow aloft, the outflow being enhanced by latent heating (Davis *et al.* 1993; Stoelinga 1996). In some cyclones, another factor is that latent heating influences the surface potential-temperature distribution, which in turn will alter the induced advective effects at upper levels.

It has been found that the contribution of the UPV anomaly to the low-level cyclone does not increase during intensification of the system (section 4). This may simply be

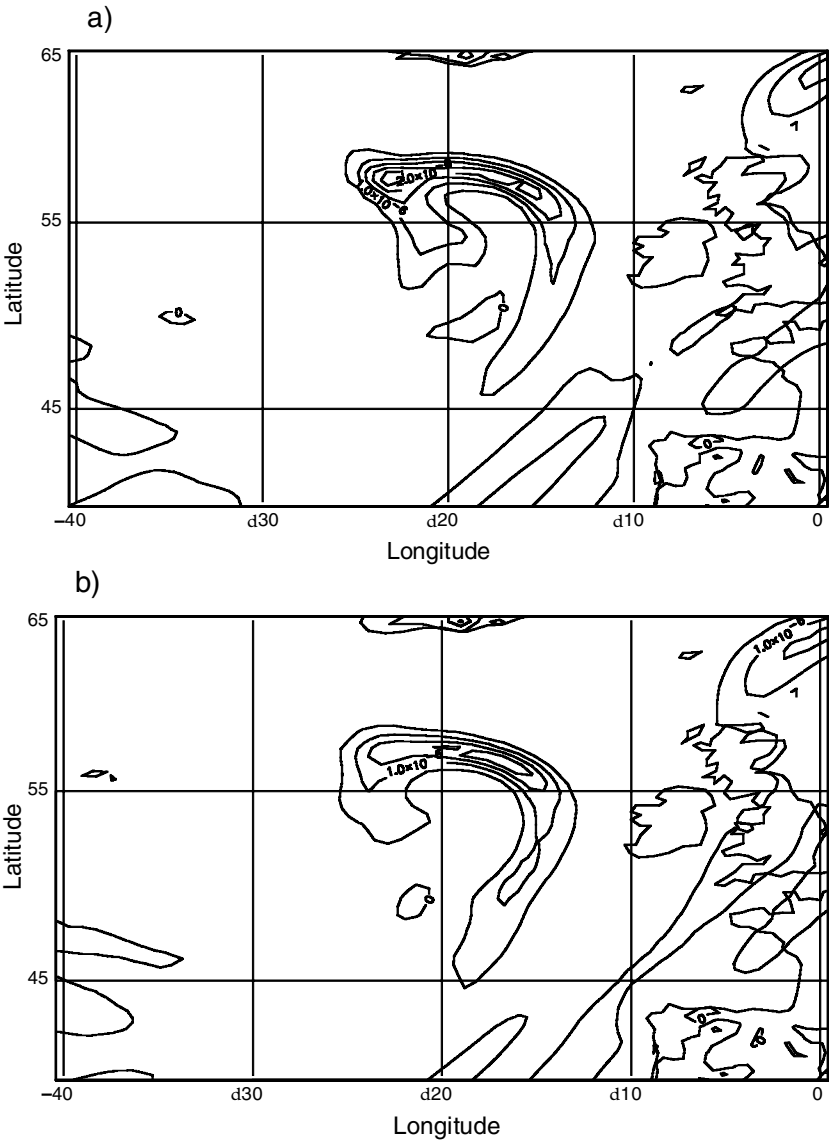

Figure 10. The PV field at 850 mb in (a) the CON1 and (b) the MLP experiments, at 1200 UTC 23 February, 12 h after the start of the integration. The contour interval is 0.5 PVU.

due to a weak impact of latent heating and weak feedback from the low-level anomalies but might also occur through cancellations between various factors.

One of the possible mechanisms is upper-level PV advection due to the winds attributed to the LPV and θ_B anomalies. In particular, consider advection along the 305 K isentropic surface. During the incipient stage, the feedback is very weak (not shown). The feedback remains moderate during intensification (Fig. 11). For example, at the time of most rapid deepening (0600 UTC 23 February), the northerly flows attributed to the LPV anomaly lie approximately parallel to the PV contours west of ~30°W (Fig. 11(b)). In the base of the trough, the attributed winds are suitably positioned

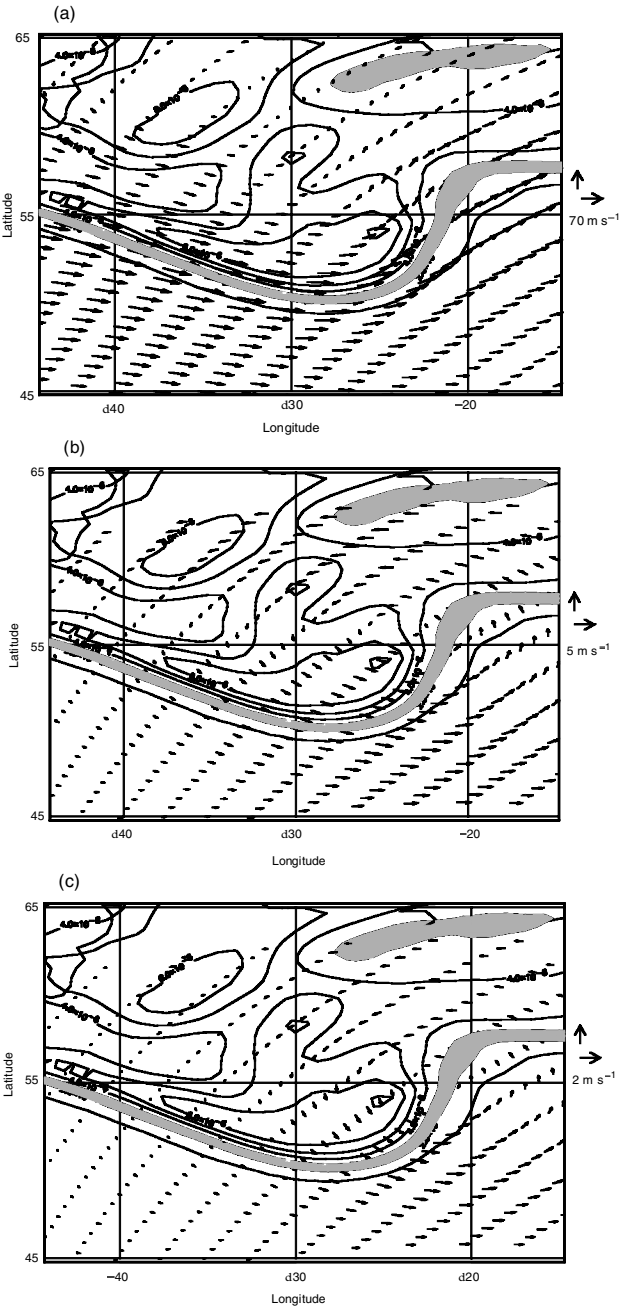

Figure 11. Potential-vorticity field on the 305 K isentropic surface at 0600 UTC 23 February with the wind vectors on that surface overlaid: (a) full winds, (b) winds attributed to the LPV anomaly, and (c) winds attributed to the θ_B anomaly. The PV contour interval is 1 PVU, with values between 2 and 3 PVU shaded. The scale for the wind vectors is shown by the arrows to the right of each panel. Note the different wind vector scales used.

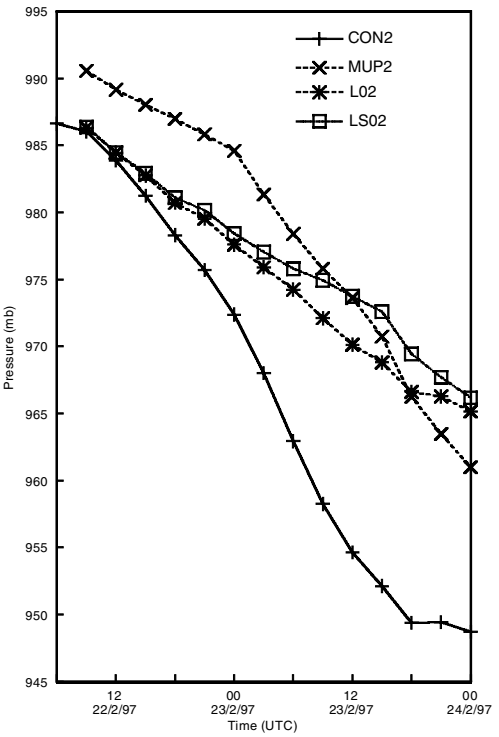

Figure 12. Time series at 3 h intervals of the minimum surface pressure of the IOP18 cyclone in control and sensitivity simulations. Each simulation is labelled by an identifer. The identifiers are listed in Table 2.

to produce southward PV advection, while the induced southerly winds may act to intensify somewhat the downstream upper-level ridge. However, the strength of these flows for both the LPV and θ_B anomalies is fairly weak. We have estimated that the attributed flow components perpendicular to the PV contours will have displaced the UPV anomaly by $\lesssim 1^\circ$ of latitude over the previous 24 h*. Comparing this to the total north–south displacement of PV that constitutes the UPV anomaly, $\sim 4^\circ$, it appears that the UPV anomaly continues its evolution with a noticeable but by no means an overwhelming level of advective feedback from the lower-level anomalies.

The cumulative effect of latent-heat release through all processes can be gauged by comparing the control simulation CON2 to the corresponding run without latent-heat release (L02; see Table 2 for description). The minimum surface pressure at T+42 reaches 949 mb in CON2 but only 965 mb in L02 (Fig. 12). Thus, latent-heat release is responsible for a substantial portion of the total deepening. PV inversions have been performed on the L02 data in order to determine the low-level fields attributable to the UPV anomaly in this case. In the absence of latent heating, the 850 mb geopotential perturbation attributed to the UPV anomaly is $\sim$30% stronger (Fig. 7). Thus, in contrast to some previous studies, which suggested mutual enhancement of upper-level and diabatically produced PV anomalies (such as Craig and Cho 1992; Reed *et al.* 1993; Stoelinga 1996), in this case latent heating has a considerable negative impact on the upper-level anomaly.

* Our estimate takes into account that the attributed flows are weaker during the previous 24 h and that the winds attributed to the thermal anomaly actually have a negative advective effect on the UPV anomaly at earlier times (Ahmadi-Givi 2001, Fig. 4.4).

Since the advective effects of the LPV and θ_B anomalies at upper levels are moderate (Fig. 11), and since latent heating does not influence upper levels significantly through adjustment of the surface thermal field*, it follows that differences in upper-level PV between the two experiments are dominated by direct, diabatic modification and enhanced divergent outflow. It may be possible to draw a distinction between the two mechanisms by diagnosing the direct impact explicitly in CON2, following perhaps the partitioned-PV-integration approach of Davis *et al.* (1993) and Stoelinga (1996). We have not attempted such an analysis here.

The effect which latent heating has on the upper-level PV through these mechanisms is shown in Fig. 13, where we compare the PV fields from CON2 and L02 at T+30. It is immediately apparent that latent heating acts to inhibit the downward penetration of the UPV anomaly and to decrease the horizontal extent of the tropopause fold. Such effects are weak initially, but become more pronounced during the intensification stage. The reductions to the vertical and horizontal extent of the anomaly will both contribute to decreases in the strength of its associated circulation (Hoskins *et al.* 1985).

An interesting feature of L02 is the occurrence at low levels of a broad region of very low PV values, close to zero (Fig. 13(b)). This is associated with near-zero static stability in the region, probably due to dry convective adjustment over a deep layer when latent heat is excluded. One might expect that this very weak low-level static stability would enhance the penetration of the fields attributable to the UPV anomaly, and thereby intensify the cyclone development. However, any effects of this nature would appear to be rather weak. If the PV inversions for L02 are repeated with the tropospheric static stability increased to the values found in the control experiment, then there is little difference in the strength of the induced low-level circulation.

As the cyclone intensifies, a small-scale upper-level ridge is formed downstream of the short-wave positive UPV anomaly (Fig. 4). We shall refer to the negative anomaly of reduced upper-level PV in the ridge as the RUPV anomaly. Since this anomaly is absent in experiment L02, it would appear that latent-heat release controls its formation. One can attempt to investigate the effects of the ridge on the low-level cyclone by performing PV inversions in which both the short-wave positive UPV anomaly and the negative RUPV anomaly are removed. However, any conclusions must be somewhat tentative because the nonlinearity of the inversion process may have some effect for anomalies that are not well separated (Birkett and Thorpe 1997). Preliminary results (Ahmadi-Givi 2001) suggest that the character of the flow attributable to the RUPV anomaly is as illustrated by Fig. 14(c). The UPV and RUPV anomalies induce cyclonic and anticyclonic circulations at the surface. Low-level southerly flow associated with the RUPV anomaly is co-located with the southerly flow induced by the UPV anomaly, thereby enhancing somewhat the flow around the cyclone centre. However, the impact of the RUPV anomaly is weak. Certainly its effect is very much weaker than the impact of latent heating on the low-level fields attributed to the UPV anomaly†.

Figure 14 summarizes the various effects of diabatic heating on the upper-level PV. Figure 14(a) shows the UPV anomaly and its associated low-level circulation in the absence of latent heating, while Fig. 14(b) depicts the negative impact of latent-heat release on the UPV anomaly by inhibiting its downward penetration and reducing its horizontal extent.

* The surface potential-temperature field is changed somewhat in experiment L02, but the feedback from the thermal anomaly to the UPV anomaly is so weak in this cyclone that such changes are of little consequence for the upper-level PV.

† This can be estimated by comparing UPV inversions from CON2 and L02, which have 850 mb geopotential-height differences of ~50 m at T+30.

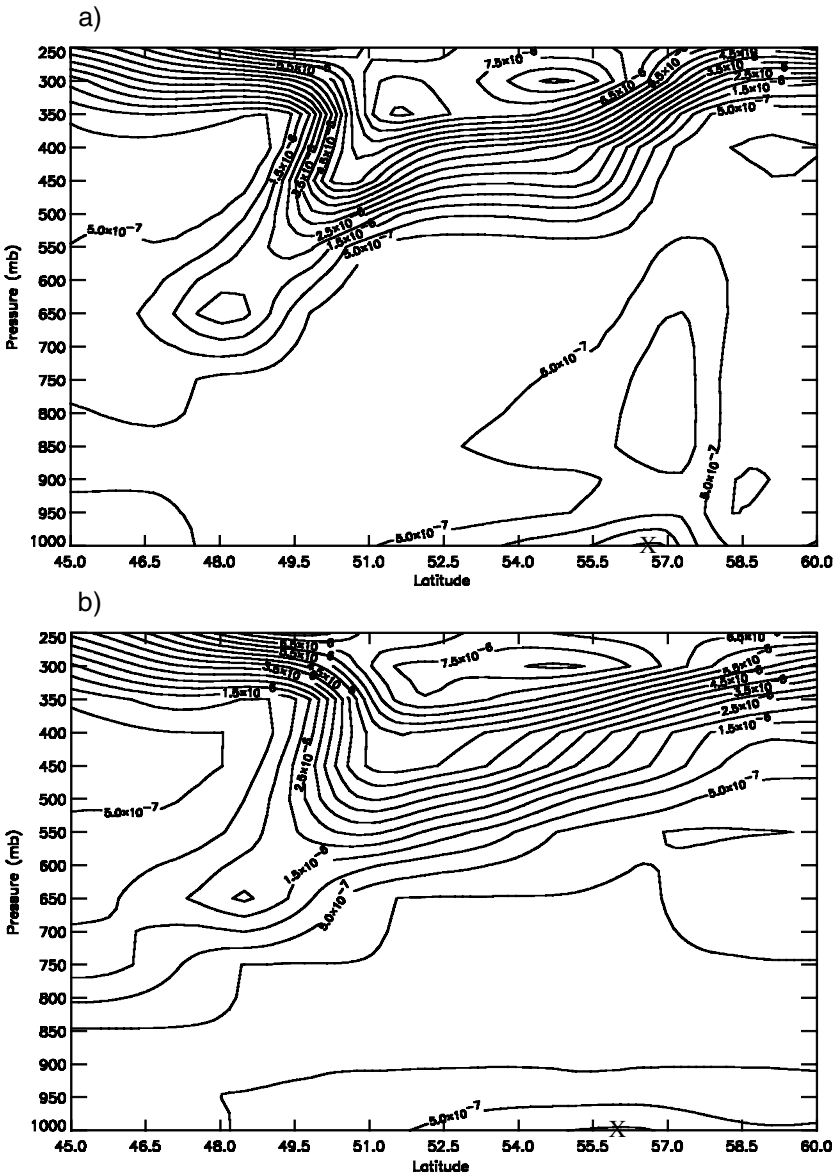

Figure 13. North–south cross-sections of potential vorticity at 1200 UTC 23 February 1997 for experiments (a) CON2 and (b) L02. The cross-sections are drawn through the longitude of the minimum surface pressure in the control experiment CON2 at this time (21.6° W). The crosses denote the latitude of minimum surface pressure at this time in each experiment. The contour interval is 0.5 PVU.

(*c*) *Evolution of the UPV anomaly*

As discussed in section 4, the low-level fields attributed to the UPV anomaly remain of approximately the same strength throughout the intensification of IOP18 (Fig. 7). In the absence of latent-heat release (experiment L02 in Fig. 12), however, Fig. 7 shows that the geopotential-height perturbations associated with the UPV anomaly actually increase over time. It would therefore appear that the lack of intensification of low-level

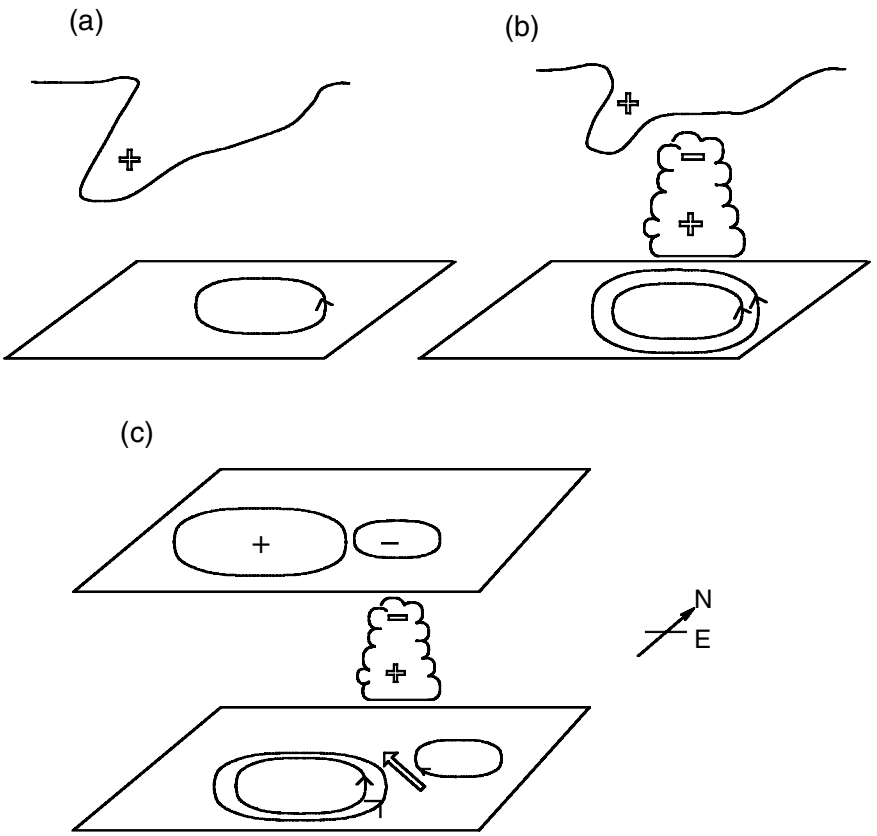

Figure 14. Schematic illustration of the various effects of latent-heat release on the low-level circulation associated with upper-level potential-vorticity anomalies. (a) The situation with no latent-heat release. The upper line denotes a tropopause fold, with associated positive PV anomaly. A low-level, cyclonic circulation is induced. (b) The dominant effects of latent heating. A positive low-level anomaly is formed which intensifies the low-level circulation. A local sink of PV is located above, and erodes the upper-level feature. (c) A subsidiary effect of latent-heat release. A downstream ridge is generated, and is associated with weak, downstream anti-cyclonic flow.

fields attributed to the UPV anomaly in the presence of latent heating must arise through a cancellation between the effects of latent-heat release at upper-levels (which act to weaken the attributed fields) and the action of upper-level processes (which must be acting to strengthen the UPV anomaly).

The intensification of synoptic disturbances through upper-level barotropic processes has been examined in a number of recent studies (Cai and Mak 1990; Swanson *et al.* 1997; Kucharski and Thorpe 2000; Lee 2000), and case-studies have sometimes shown interaction between upper-level PV anomalies to be important in cyclogenesis (Hakim *et al.* 1996; Huo *et al.* 1999; Chaigne and Arbogast 2000), but it is difficult to identify the precise causes of the upper-level amplification of the IOP18 cyclone. As described in section 3, the UPV anomaly is first distinguished as an elongated anomaly (Fig. 4(a)) located upstream of the axis of a major, large-scale, upper-level trough. Over time, the UPV anomaly moves south-eastward relative to the large-scale trough, reaching its base around 0600 UTC 23 February (Fig. 4(b)). Simple linear superposition of the UPV anomaly with the large-scale PV trough would lead to an enhanced

cyclonic perturbation at the surface, but there is also the possibility of nonlinear interactions between the short-wave and long-wave anomalous structures that might produce a localized amplification of the UPV anomaly. Sequences of PV maps on isentropic surfaces (not shown) reveal that the horizontal deformation increases markedly on the upstream side of the main trough, and that the zonal scale of the trough is reduced in the period when the surface cyclone intensifies, features which may be associated with a more intense low-level circulation (Hoskins *et al.* 1985).

6. Conclusions

The role of latent-heat release in the explosively developing FASTEX IOP18 cyclone has been investigated. This system is one for which convection and latent-heat release are particularly strong throughout the development of the storm. The dynamics of the case can be compared to those predicted by baroclinic instability theory, albeit in a form modified to attempt to account for latent-heating effects. This conventional view of cyclone development is summarized from the PV perspective by Fig. 1, in which the main effect of latent heating is seen to be the addition of a positive PV anomaly in the lower troposphere, positioned so as to enhance the effects of the surface thermal anomaly.

A synoptic analysis indicates that the development of the system is comprised of three main stages. During the incipient stage, an upper-level PV anomaly can be identified, but there is only a very weak surface thermal perturbation. In the intensification stage, both a surface thermal anomaly and low-level PV anomaly develop, and reach their maximum intensity at the beginning of the final, mature stage. The strength of the upper-level anomaly did not change significantly throughout this time. PV inversions show that the contribution of the surface thermal anomaly to the deepening of the cyclone is very weak in comparison with the contributions from the other identified anomalies (Fig. 7). During the intensifying stage, the LPV anomaly amplifies dramatically, and eventually the UPV and LPV anomalies contribute to the system to a comparable extent. Numerical experiments confirm that the UPV anomaly is crucial for the initiation of the system, that the LPV anomaly is responsible for much of the intensification of the system and that the thermal anomaly is almost irrelevant (Figs. 8 and 12). This life cycle, consisting of an interaction between the UPV and the diabatically generated LPV anomalies, is quite different from the conventional picture of a midlatitude cyclone.

Numerical sensitivity tests reveal that the LPV anomaly is generated through rapid processes of latent-heat release, consistent with the findings of Stoelinga (1993) and Pomroy and Thorpe (2000). Surface heat fluxes had only a small effect on the generation of the LPV anomaly. Generation of the weak θ_B anomaly may be attributed roughly equally to the circulations induced by the UPV and LPV anomalies. Advective feedbacks from the lower-level PV anomalies on the upper-level PV did occur but were found to be weak relative to other effects of latent heating on the upper-level PV.

The primary effects of latent-heat release on the upper-level PV arise from a direct, diabatic reduction of PV and enhancement of the divergent outflow aloft. Simulations without latent-heat release indicated that these processes acted to reduce both the downward penetration and the horizontal extent of the UPV anomaly (Fig. 14(b)), leading to a significant decrease in the strength of the low-level fields attributed to the UPV anomaly. This result may be contrasted with some other systems (Craig and Cho 1992; Reed *et al.* 1993; Stoelinga 1996), in which there is a mutual enhancement between upper-level and diabatic PV anomalies. An additional product of latent-heat

release is an upper-level ridge, downstream of the short-wave, positive UPV anomaly. The ridge appears to have some positive, albeit minor, impact on the low-level cyclone by enhancing the southerly flow (Fig. 14(c)).

Another interesting aspect of this cyclone, not explored in detail here, was the amplification of the UPV anomaly in the absence of both latent heating and a significant surface thermal anomaly. This may be due to barotropic growth or the interaction of the localized UPV anomaly with the large-scale trough in which it was embedded.

The evolution of the IOP18 cyclone can be encapsulated as the interaction of a short-wave, upper-level PV anomaly with a weak, low-level baroclinic zone. Although the low-level thermal gradient was too weak to produce a significant surface thermal anomaly, there was sufficient moisture available to produce substantial diabatic heating. Diabatic PV production led to a large-amplitude, low-level PV anomaly that accounted for much of the growth of the surface cyclone. Diabatic effects also acted both directly and indirectly to weaken the upper-level anomaly. This development may be quite different from the conventional picture of midlatitude cyclogenesis, but nevertheless there are reasons for believing that it may represent more than an unusual, isolated case. Using height-attributable, quasi-geostrophic, vertical-motion diagnostics, Deveson *et al.* (2002) have attempted to construct an objective method for identifying the Type A and Type B cyclone classes of Petterssen and Smebye (1971). Of the sixteen FASTEX cyclones considered, three systems (including the IOP18 cyclone) did not fit the Type A and Type B categories, and were assigned the category Type C. Characteristics of type C include the dominant initial role of an upper-level feature, the persistently weak influence of surface thermal anomalies, and the increase of westward tilt with height as the cyclone intensifies. We intend to discuss these characteristics further, and their relationship to the dynamics described here, in a forthcoming paper (Plant *et al.* 2003).

Acknowledgements

The authors wish to thank M. Griffiths for the use of her PV inversion code and H. Pomroy for useful discussions on PV inversion. Thanks are also due to P. Panagi and E. Dicks from the Joint Centre for Mesoscale Meteorology, Reading for supplying LAM data used here. F. Ahmadi-Givi acknowledges support by a scholarship from the Iranian Ministry of Science, Research and Technology. R. Plant acknowledges funding from the Universities Weather Research Network programme, supported by the Natural Environment Research Council.

References

Adamson, D. S. 2001 'Boundary layer frictional processes in mid-latitude cyclones'. PhD thesis, University of Reading

Ahmadi-Givi, F. 2001 'The role of latent heat release in an explosive extratropical cyclogenesis'. PhD thesis, University of Reading

Bader, M. J., Forbes, G. S., Grant, J. R., Lilley, R. B. E. and Waters, A. J. 1995 *Images in weather forecasting*. Cambridge University Press

Balasubramanian, G. B. and Yau, M. K. 1994 The effects of convection on a simulated marine cyclone. *J. Atmos. Sci.*, **51,** 2397–2417

1996 The life cycle of a simulated marine cyclone: Energetics and potential vorticity diagnostics. *J. Atmos. Sci.*, **53,** 639–653

Birkett, H. R. and Thorpe, A. J. 1997 Superposing semi-geostrophic potential-vorticity anomalies. *Q. J. R. Meteorol. Soc.*, **123,** 2157–2163

Bishop, C. and Thorpe, A. J. 1994 Potential vorticity and the electrostatics analogy: Quasi-geostrophic theory. *Q. J. R. Meteorol. Soc.*, **120,** 713–731

Browning, K. A. 1995 'Mesoscale aspects of extratropical cyclones: An observational perspective'. Internal Report No. 44, Joint Centre for Mesoscale Meteorology, Reading, UK

Cai, M. and Mak, M. 1990 On the basic dynamics of regional cyclogenesis. *J. Atmos. Sci.*, **47,** 1417–1442

Chaigne, E. and Arbogast, P. 2000 Multiple potential-vorticity inversions in two FASTEX cyclones. *Q. J. R. Meteorol. Soc.*, **126,** 1711–1734

Charney, J. G. 1955 The use of the primitive equations of motion in numerical prediction. *Tellus*, **7,** 22–26

Clough, S. A. and Davitt, C. S. A. 1994 'Development of an Atlantic frontal wave during IOP3 of FRONTS92'. Pp. 151–156 in *The life cycles of extratropical cyclones,* Vol. II. Proceedings of an international symposium, 27th June–1st July 1994, University of Bergen. Eds. S. Grønas and M. A. Shapiro. American Meteorological Society, 45 Beacon Street, Boston MA02108-3693, USA

Clough, S. A., Lean, H. W., Roberts, N. M., Birkett H., Chaboureau, J.-P., Dixon, R., Griffiths, M., Hewson, T. D. and Montani, A. 1998 'A JCMM overview of FASTEX IOPs'. Internal Report No. 81, Joint Centre for Mesoscale Meteorology, Reading, UK

Craig, G. C. and Cho, H. R. 1988 Cumulus convection and CISK in the extratropical atmosphere. Part I: Polar lows and comma clouds. *J. Atmos. Sci.*, **45,** 2622–2640

1992 Cumulus convection and CISK in midlatitudes. Part II: Comma cloud formation in cyclonic shear regions. *J. Atmos. Sci.*, **49,** 1318–1333

Cullen, M. J. P. 1993 The unified forecast/climate model. *Meteorol. Mag.*, **122,** 89–94

Danard, M. B. 1964 On the influence of released latent heat on cyclone development. *J. Appl. Meteorol.*, **3,** 27–37

Davis, C. A. 1992 A potential vorticity diagnosis of the importance of initial structure and condensational heating in observed extratropical cyclogenesis. *Mon. Weather Rev.*, **120,** 2409–2428

Davis, C. A. and Emanuel, K. A. 1991 Potential vorticity diagnostics of cyclogenesis. *Mon. Weather Rev.*, **119,** 1929–1953

Davis, C. A., Stoelinga, M. T. and Kuo, Y.-H. 1993 The integrated effect of condensation in numerical simulations of extratropical cyclogenesis. *Mon. Weather Rev.*, **121,** 2309–2330

Deveson, A. C. L., Browning, K. A. and Hewson, T. D. 2002 A classification of FASTEX cyclones using a height-attributable quasi-geostrophic vertical-motion diagnostic. *Q. J. R. Meteorol. Soc.*, **128,** 93–118

Emanuel, K. A., Fantini, M. and Thorpe, A. J. 1987 Baroclinic instability in an environment of small stability to slantwise moist convection. Part I: Two-dimensional models. *J. Atmos. Sci.*, **44,** 1559–1573

Fehlmann, R. and Davies, H. C. 1998 Role of salient PV-elements in an event of frontal wave cyclogenesis. *Q. J. R. Meteorol. Soc.*, **124,** 1–22

Griffiths, M., Thorpe, A. J. and Browning, K. A. 2000 Convective destabilization by a tropopause fold diagnosed using potential-vorticity inversion. *Q. J. R. Meteorol. Soc.*, **126,** 125–144

Gyakum, J. R. 1983a On the evolution of the QE II storm. I: Synoptic aspects. *Mon. Weather Rev.*, **111,** 1137–1155

1983b On the evolution of the QE II storm. II: Dynamic and thermodynamic structure. *Mon. Weather Rev.*, **111,** 1156–1173

Hakim, G. J., Keyser, D. and Bosart, L. F. 1996 The Ohio Valley wave-merger cyclogenesis event of 25–26 January 1978. Part II: Diagnosis using quasigeostrophic potential vorticity inversion. *Mon. Weather Rev.*, **124,** 2176–2205

Harrold, T. W. 1973 Mechanisms influencing the distribution of precipitation within baroclinic disturbances. *Q. J. R. Meteorol. Soc.*, **99,** 232–251

Hoskins, B. J. and Berrisford, P. 1988 A potential-vorticity perspective of the storm of 15–16 October 1987. *Weather*, **43,** 122–129

Hoskins, B. J., McIntyre, M. E. and Robertson, A. W. 1985 On the use and significance of isentropic potential vorticity maps. *Q. J. R. Meteorol. Soc.*, **111,** 877–946

Huo, Z., Zhang, D. L. and Gyakum, J. R. 1999 Interaction of potential vorticity anomalies in extratropical cyclogenesis. Part I: Static piecewise inversion. *Mon. Weather Rev.*, **127,** 2546–2561

Joly, A., Jorgensen, D., Shapiro, M. A., Thorpe, A. J., Bessemoulin, P., Browning, K. A., Cammas, J. P., Chalon, J.-P., Clough, S. A., Emanuel, K. A., Eymard, L., Gall, R., Hildebrand, P. H., Langland, R. H., Lemaitre, Y., Lynch, P., Moore, J. A., Persson, P. O. G., Snyder, C. and Wakimoto, R. M.	1997	Definition of the Fronts and Atlantic Storm-Track Experiment (FASTEX). *Bull. Am. Meteorol. Soc.*, **78,** 1917–1940
Kucharski, F. and Thorpe, A. J.	2000	Upper-level barotropic growth as a precursor to cyclogenesis during FASTEX. *Q. J. R. Meteorol. Soc.*, **126,** 3219–3232
Kuo, Y.-H., Shapiro, M. A. and Donall, E. G.	1991a	The interaction of baroclinic and diabatic processes in a numerical simulation of a rapidly intensifying extratropical marine cyclone. *Mon. Weather Rev.*, **119,** 368–384
Kuo, Y.-H., Reed, R. J. and Low-Nam, S.	1991b	Effects of surface energy fluxes during the early development and rapid intensification stages of seven explosive cyclones in the western Atlantic. *Mon. Weather Rev.*, **119,** 457–476
	1992	Thermal structure airflow in a model simulation of an occluded marine cyclone. *Mon. Weather Rev.*, **120,** 2280–2297
Lee, S.	2000	Barotropic effects on atmospheric storm tracks. *J. Atmos. Sci.*, **57,** 1420–1435
Macpherson, B., Wright, B. J., Hand, W. H. and Maycock, A. J.	1996	The impact of MOPS moisture data in the UK Meteorological Office mesoscale data simulation scheme. *Mon. Weather Rev.*, **124,** 1746–1766
Montgomery, M. T. and Farrell, B. F.	1991	Moist surface frontogenesis associated with interior potential vorticity anomalies in a semi-geostrophic model. *J. Atmos. Sci.*, **48,** 343–367
Panagi, P. and Dicks, E.	1997	'Met. Office Unified Model, diagnostic, graphics programs, and other observational data available from the JCMM through the aegis of the Universities Weather Research Network (plus Supplement)'. Internal Report No. 69, Joint Centre for Mesoscale Meteorology, Reading, UK
Parker, D. J. and Thorpe, A. J.	1995	Conditional convective heating in a baroclinic atmosphere: A model of convective frontogenesis. *J. Atmos. Sci.*, **52,** 1699–1711
Persson, P. O. G.	1995	Simulations of the potential vorticity structure and budget of FRONTS 87 IOP8. *Q. J. R. Meteorol. Soc.*, **121,** 1041–1081
Petterssen, S. and Smebye, S. J.	1971	On the development of extratropical cyclones. *Q. J. R. Meteorol. Soc.*, **97,** 457–482
Plant, R. S., Craig, G. C. and Gray, S. L.	2003	On a threefold classification of extratropical cyclogenesis. *Q. J. R. Meteorol. Soc.*, **129,** 2989–3012
Pomroy, H. R. and Thorpe, A. J.	2000	The evolution and dynamical role of reduced upper-tropospheric potential vorticity in intensive observing period one of FASTEX. *Mon. Weather Rev.*, **128,** 1817–1834
Reed, R. J., Stoelinga, M. T. and Kuo, Y.-H.	1992	A model-aided study of the origin and evolution of the anomalously high potential vorticity in the inner region of a rapidly deepening marine cyclone. *Mon. Weather Rev.*, **120,** 893–913
Reed, R. J., Grell, G. A. and Kuo, Y.-H.	1993	The ERICA IOP5 Storm. Part II: Sensitivity tests and further diagnosis based on model output. *Mon. Weather Rev.*, **121,** 1595–1612
Shapiro, M. A. and Keyser, D.	1990	'Fronts, jet streams and the tropopause.' Pp. 167–191 in *Extratropical cyclones. The Eric Palmen Memorial Volume.* American Meteorological Society, 45 Beacon Street, Boston MA02108-3693, USA
Snyder, C. and Lindzen, R.	1991	Quasi-geostrophic wave-CISK in an unbounded baroclinic shear. *J. Atmos. Sci.*, **48,** 76–86
Stoelinga, M. T.	1993	'Assessing the role of frictional and diabatic processes in a numerically simulated frontal cyclone using potential vorticity analysis'. PhD thesis, University of Washington
	1996	A potential vorticity-based study of the role of diabatic heating and friction in a numerically simulated baroclinic cyclone. *Mon. Weather Rev.*, **121,** 849–874
Swanson, K. L., Kushner, P. J. and Held, I. M.	1997	Dynamics of barotropic storm tracks. *J. Atmos. Sci.*, **54,** 791–810

Tracton, M. S. 1973 The role of cumulus convection in the development of extratropical cyclones. *Mon. Weather Rev.*, **101,** 573–592

Wernli, H. and Davies, H. C. 1997a A Lagrangian-based analysis of extratropical cyclones. I: The method and some applications. *Q. J. R. Meteorol. Soc.*, **123,** 467–489

1997b A Lagrangian-based analysis of extratropical cyclones. II: A detailed case-study. *Q. J. R. Meteorol. Soc.*, **123,** 1677–1706

Whitaker, J. S. and Davis, C. A. 1994 Cyclogenesis in a saturated environment. *J. Atmos. Sci.*, **51,** 889–907

Young, M. V., Monk, G. A. and Browning, K. A. 1987 Interpretation of satellite imagery of a rapidly deepening cyclone. *Q. J. R. Meteorol. Soc.*, **113,** 1089–1115